P-ISSN 1991-8941
E-ISSN 2706-6703
Vol. 20, No. 2 (2026)

Journal of University of Anbar for Pure Science
(JUAPS)

journal homepage: juaps.uoanbar.edu.iq

Open Access

Original Paper

Improving the electrochemical performance of lithium- and manganese-rich layered cathodes through low-level zinc doping

Rafed Jawad Khadem[1*]

[1]Faculty of Physics, Department of Condensed Matter Physics, University of Isfahan, Iran

ARTICLE INFO

Received: 04/09/2025
Revised: 26/11/2025
Accepted: 08/01/2026
Available online: 08/08/2026
August Issue
10.37652/juaps.2026.164769.1664

Cite @ JUAPS

Corresponding author
Rafed Jawad Khadem
rafedjawad688@gmail.com

ABSTRACT

In this study, Li $[Li_{0.20}Mn_{0.54}Ni_{0.13}Co_{0.13-x}Zn_x]\,O_2$ samples with zinc doping levels of x = 0, 0.02, and 0.05 were synthesized using the sol-gel method. Structural characterization was performed using field-emission scanning electron microscopy (FESEM), Fourier-transform infrared spectroscopy (FTIR), Raman spectroscopy, and X-ray diffraction (XRD). The results showed that partial substitution with zinc increased the lattice parameters and reduced the crystallite size. Notably, the layered crystal structure remained unchanged, retaining the α $NaFeO_2$ structure. These structural modifications improved lithium-ion transport without significantly altering the overall morphology. Electrochemical evaluation revealed that zinc doping improved charge-transfer kinetics and cycling stability. Cyclic voltammetry showed sharper and more intense redox peaks, indicating reduced polarization. Electrochemical impedance spectroscopy demonstrated a decrease in charge-transfer resistance from 317.4Ω for the undoped sample to 135Ω and 118Ω for the doped compositions. Galvanostatic charge-discharge tests showed that zinc doping increased the discharge capacity to 283.6 and 298.7 $mAhg^{-1}$ compared with 249.8$mAhg^{-1}$ for the undoped material, while also improving Coulombic efficiency. These findings confirm that minor zinc substitution can enhance structural stability and reduce interfacial resistance, suggesting a promising approach for improving the electrochemical performance, energy density, and cycling life of lithium-ion battery cathode materials.

Keywords: *Electrochemical performance, Energy storage, Lithium-ion battery, Lithium and manganese-rich layered cathode, Zn doping*

1 INTRODUCTION

The urgent need to reduce fossil fuel consumption and address climate change has increased global demand for sustainable and efficient energy-storage systems. Although renewable energy sources, such as solar and wind power, are rapidly expanding, their intermittent nature requires reliable, high-performance rechargeable batteries that can consistently store and deliver energy. Owing to their high energy density, long operational lifespan, and favorable charge–discharge characteristics, lithium-ion batteries (LIBs) have become a leading technology for portable electronic devices, electric vehicles, and large-scale energy-storage systems [1, 2]. Despite their success, conventional LIB chemistries still face several challenges in meeting the performance requirements of advanced applications. Common limitations include capacity degradation during long-term cycling, slow lithium-ion diffusion kinetics, and cathode instability at high operating voltages [3, 4]. Because the cathode is a key determinant of energy density and cycling stability, improving cathode performance is essential for enabling LIBs to meet the demands of applications such as electric mobility and aerospace systems [5, 6].

Lithium- and manganese-enriched layered oxides,

This is an open-access article under CC BY 4.0

© 2026 *The Author(s).* Published by College of Science, University of Anbar.

represented as $Li_{1+x}M_{1-x}O_2$, where M generally represents Mn, Ni, or Co, are regarded as promising cathode materials. These materials exhibit high reversible capacities exceeding $250mAhg^{-1}$ and energy densities higher than those of conventional $LiCoO_2$ cathodes [7]. Their layered $\alpha - NaFeO_2$ structure with the R-3m space group provides well-defined lithium-ion diffusion pathways [8]. These advantages have encouraged research on Li $[Li_{0.20}Mn_{0.54}Ni_{0.13}Co_{0.13}]$ O_2 cathode materials. In this context, Hendrickx et al. investigated the effect of synthesis method on the structure and electrochemical performance of Li-rich/Mn-rich NMC cathodes. Their study showed that cathodes prepared by the sol-gel method exhibited greater capacity decay than those synthesized by the coprecipitation method, which was attributed to the smaller particle size of the cathode material [9].

Despite their advantages, lithium- and manganese-enriched layered oxides still suffer from several limitations, including voltage decay, structural instability, and oxygen loss during cycling, which restrict their practical application [10]. Cationic substitution, or doping, is a widely used strategy to overcome these drawbacks. Partial replacement of transition-metal sites with heteroatoms can stabilize the layered framework, suppress undesirable phase transitions, and enhance lithium-ion transport [6, 11]. Among potential dopants, zinc (Zn) offers specific advantages because of its larger ionic radius compared with cobalt (Co) and nickel (Ni). Zinc substitution can slightly expand the lattice, improve lithium-ion diffusion, and reduce polarization during cycling [12, 13]. Moreover, Zn is electrochemically inactive within the operating voltage range, which may contribute to structural stability without participating in redox reactions. In addition, unlike Co, Zn is abundant and relatively non-toxic. The subtle lattice changes induced by Zn substitution may also help mitigate oxygen release during high-voltage operation, a process often associated with irreversible capacity loss and safety concerns. By improving structural robustness and reducing side reactions with the electrolyte, Zn doping may extend the cycling life of LIBs in demanding applications, including grid storage and aerospace missions, where reliability is essential.

Previous studies have shown that even small amounts of Zn addition can improve electronic conductivity, reduce charge-transfer resistance, and enhance high-rate cycling performance [12, 14]. In this study, we aimed to elucidate the effect of low-level Zn doping, with x = 0.02 and 0.05 in Li $[Li_{0.20}Mn_{0.54}Ni_{0.13}Co_{0.13-x}Zn_x]$ O_2, on the structural, morphological, and electrochemical characteristics of lithium- and manganese-rich layered cathodes. To the best of our knowledge, limited studies have examined the effect of different Zn dopant concentrations on both the structure and electrochemical performance of lithium-manganese-rich layered cathodes. Therefore, in this study, structural modifications and electrochemical behavior were investigated using complementary characterization and electrochemical techniques.

2 MATERIALS AND METHODS

2.1 Synthesis of pure nanopowder

All chemicals used in this study were of analytical grade and were purchased from Merck. For the synthesis of the pure nanopowder, precise quantities of metal salts were weighed according to the required stoichiometric ratio. The starting materials included 1.298 g of nickel nitrate hexahydrate $[Ni(NO_3)_2 \cdot 6H_2O]$, 1.3 g of cobalt nitrate hexahydrate $[Co(NO_3)_2 \cdot 6H_2O]$, 4.73 g of manganese nitrate tetrahydrate $[Mn(NO_3)_2 \cdot 4H_2O]$, and 3.008 g of lithium nitrate $[LiNO_3]$. Double-distilled water was used as the solvent to dissolve all components and obtain a clear homogeneous solution. The mixture was then placed in an oil bath maintained at 75-80 °C under continuous stirring. Heating and stirring were continued until all ionic components were completely dissolved and uniformly distributed throughout the solution.

Subsequently, 13.52 g of citric acid was added as a chelating and crosslinking agent, and stirring was continued until a homogeneous gel was formed. The gelation process was maintained at 80°C for approximately 4 h to ensure the formation of a stable gel matrix. The obtained gel was then dried in an oven at 120 °C for 6 h. A precalcination step was subsequently performed at 150 °C for 5 h, followed by calcination at 850 °C for 4 h in air to obtain a stable crystalline phase. The final product was obtained as a uniform black powder, indicating the formation of the desired structure [7].

2.2 Synthesis of zinc-doped nanopowder

The zinc-doped samples were synthesized using a procedure similar to that used for the pure sample, except that part of the cobalt in the chemical formula was replaced with zinc nitrate hexahydrate $[Zn(NO_3)_2 \cdot 6H_2O]$. Two molar ratios, x = 0.02 and x = 0.05, were selected to obtain different zinc-doping levels.

In the first step, all metal salts, including nickel nitrate, manganese nitrate, lithium nitrate, cobalt nitrate, and zinc

© 2026 *The Author(s).*

CC BY 4.0

nitrate, were dissolved in distilled water according to the required stoichiometric ratios. The cobalt nitrate amount was proportionally reduced according to the zinc content. The resulting solution was heated in an oil bath at 75-80 °C under continuous stirring. After complete dissolution, citric acid was added in the same amount used for the undoped sample. Stirring was continued until a uniform viscous gel was obtained. After 4 h of mild heating at the same temperature, the gel was dried in an oven at 120 °C for 6 h. The dried gel was then precalcined at 150 °C for 5 h and finally calcined at 850 °C for 4 h. The resulting products were obtained as uniform black powders, indicating the successful formation of stable crystalline structures at the two zinc-doping concentrations [12].

2.3 Electrochemical measurements

Electrochemical measurements were performed using CR2032 coin-type half-cells. The prepared cathode materials were used as the working electrodes, and lithium foil was used as the counter/reference electrode. The electrolyte was 1M$LiPF_6$ dissolved in ethylene carbonate/dimethyl carbonate (EC/DMC, 1:1 v/v). A microporous polypropylene membrane (Celgard 2400) was used as the separator between the working electrode and the lithium foil.

The working electrodes were prepared by casting a slurry onto aluminum foil. The slurry consisted of active material, polyvinylidene fluoride (PVDF), and carbon black at mass ratios of 85%, 5%, and 10%, respectively, dispersed in an appropriate amount of N-methyl-2-pyrrolidone (NMP). The prepared electrodes were then dried in a vacuum oven at 120 °C for 12 h.

Cyclic voltammetry (CV), electrochemical impedance spectroscopy (EIS), and galvanostatic charge-discharge measurements were performed at room temperature. CV measurements were conducted over a potential range of $2.0-5.0$ V versus $Li^{-}Li^{+}$at a scan rate of $0.5 mV s^{-1}$. EIS measurements were performed using an AC amplitude of 10 mV over a frequency range of 100 kHz to 0.1 Hz . CV and EIS analyses were carried out using a Galvanostat/Potentiostat Autolab system (PG-STAT 302N). Galvanostatic charge–discharge measurements were performed over a voltage range of $1.8-4.8$ V versus Li/Li^{+} at a rate of 0.1 C using a battery tester (Neware multichannel instrument, CT-3008).

3 RESULTS AND DISCUSSION

3.1 Characterisation tests

The crystalline structure of the synthesized cathode powders was analyzed using X-ray diffraction (XRD). This technique provides valuable information about phase formation, crystallite size, and lattice parameters. Figure 1 shows the XRD patterns of the undoped and Zn-doped cathode materials.

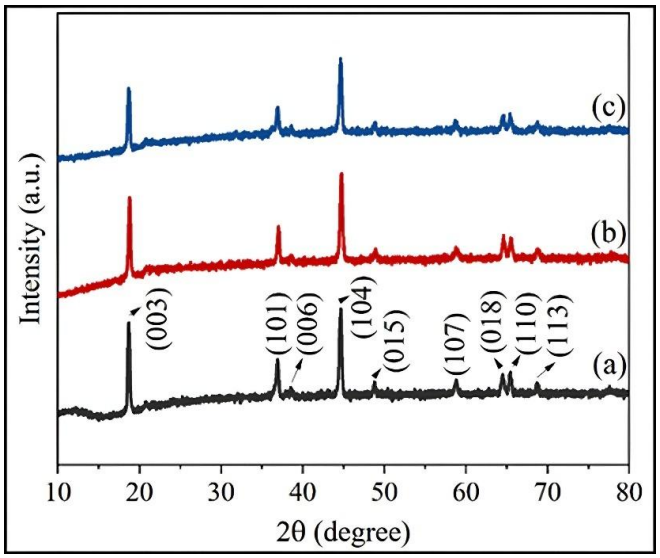

Fig. 1 X-ray diffractograms of (a) dopant-free $Li^{-}\left[Li_{0.20}Mn_{0.54}Ni_{0.13}Co_{0.13-x}Zn_x\right]O_2$ cathode (x = 0) and the ones doped with Zn where (b) x = 0.02 and (c) x = 0.05.

Based on Figure 1a, which shows the XRD pattern of the undoped Li $[Li_{0.20}Mn_{0.54}Ni_{0.13}Co_{0.13}]O_2$ cathode recorded over the 2θ range of 10°-80°, several distinct diffraction peaks were observed at approximately 18.6°, 36.9°, 38.7°, 44.6°, 48.8°, 58.8°, 64.5°, 65.4°, and 68.6°. In agreement with JCPDS file No. 49-0524, these major peaks are assigned to the (003), (101), (006), (104), (015), (107), (018), (110), and (113) crystal planes, respectively. The diffraction peaks of the undoped Li-rich NMC cathode indicate the formation of a layered $\alpha - NaFeO_2$ structure with the R-3m space group [3,4]. Figure 1b presents the XRD pattern of the Zn -doped Li $[Li_{0.20}Mn_{0.54}Ni_{0.13}Co_{0.13-x}Zn_x]O_2$ cathode with x = 0.02. The diffraction peaks corresponding to the (003), (101), (006), (104), (015), (107), (018), (110), and (113) planes, which were observed in the undoped sample, were also detected in the Zn-doped sample. No obvious peak shift was observed after Zn doping.

© 2026 *The Author(s).*

CC BY 4.0

However, a slight decrease in the intensity of some diffraction peaks, including those corresponding to the (003), (101), and (107) planes, was observed. Similarly, for the Zn-doped Li $[Li_{0.20}Mn_{0.54}Ni_{0.13}Co_{0.13-x}Zn_x]\ O_2$ cathode with x = 0.05, shown in Figure 1c, the major peaks observed in Figure 1a were also present. No clear shift in diffraction peak positions was detected, while the peak intensities showed a slight decrease. The crystallite size of the undoped and Zn-doped cathode powders was calculated using the Debye-Scherrer equation, as follows [15, 16]:

$$D = K\lambda/\beta \cos\theta (1)$$

where D represents the crystallite size, K is the Scherrer constant with a value of 0.98, λ is the X -ray wavelength (λ = 0.15418 nm), θ is the Bragg angle, and β is the full width at half maximum (FWHM). As shown in Table 1, the undoped Li-rich cathode had an average crystallite size of 35.3 nm , which was larger than those of the Zn-doped samples. Therefore, Zn doping reduced the crystallite size. However, Rietveld refinement results shown in Table 1 indicated that Zn doping slightly increased the lattice parameters a and c. This lattice expansion may enhance Li^+ diffusion and improve intercalation/deintercalation kinetics.

Table 1 The crystallite size and *a* and *c* values of the undoped Li-rich cathode of $Li[Li_{0.20}Mn_{0.54}Ni_{0.13}Co_{0.13-x}Zn_x]O_2$ (x = 0) and the ones doped with different amounts of Zn dopant. The Rietveld refinement calculations were carried out by X'Pert Highscore Plus Software.

Sample	Crystallite size (nm)	Lattice parameters		*c*/*a* ratio
		a (Å)	*c* (Å)	
Pure	35.3	2.8439	14.2128	4.9976
Pure + Zn (x = 0.02)	26.8	2.8444	14.2133	4.9969
Pure + Zn (x = 0.05)	23.1	2.8451	14.2141	4.9959

Compared with the undoped cathode material Li $[Li_{0.20}Mn_{0.54}Ni_{0.13}Co_{0.13}]\ O_2$, the Zn -doped cathodes, Li $[Li_{0.20}Mn_{0.54}Ni_{0.13}Co_{0.13-x}Zn_x]\ O_2$, exhibited increased a and c lattice parameters. This indicates that Zn doping effectively expanded the lattice dimensions. The enlarged crystalline lattice may enhance Li^+diffusion kinetics by providing greater space for intercalation and deintercalation, thereby contributing positively to the electrochemical performance of the battery [6, 12]. As shown in Table 1, the c/a ratio of all examined samples was higher than 4.99, confirming the formation of a well-defined layered structure.

Fourier-transform infrared spectroscopy (FTIR) was used as an additional characterization technique to analyze the metal-oxygen bonds in the synthesized cathode powders. Figure 2 shows the FTIR spectra of the undoped Li $[Li_{0.20}Mn_{0.54}Ni_{0.13}Co_{0.13}]\ O_2$ cathode and its Zn -doped counterparts with different Zn concentrations.

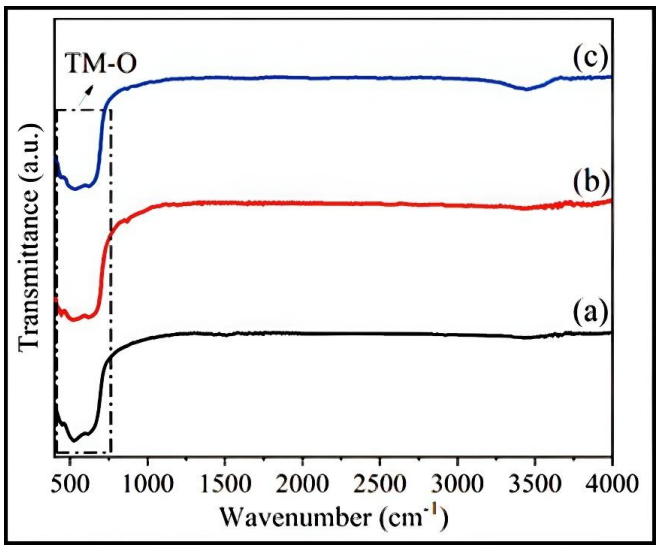

Fig. 2 FTIR spectra of (a) the undoped $Li[Li_{0.20}Mn_{0.54}Ni_{0.13}Co_{0.13-x}Zn_x]O_2$ cathode (x = 0) and those doped with Zn, where (b) x = 0.02 and (c) x = 0.05.

According to Figure 2a, which shows the FTIR spectrum of the undoped lithium-rich cathode, several absorption bands are observed at approximately 500 cm^{-1}. Based on the literature, absorption bands associated with metal-oxygen bonds are typically detected within the spectral range of 400 − 800 cm^{-1} [11, 12]. Therefore, the absorption bands observed around 500 cm^{-1} can be assigned to the vibrational modes of transition metal-oxygen (TM-O) bonds, where TM refers to the transition metals present in the cathode structure. No additional spectral peaks, other than those related to TM-O bonds, were observed in the FTIR spectrum of the undoped sample.

The incorporation of Zn dopant into the cathode structure resulted in changes in the FTIR spectral profile. As shown in Figure 2b, which presents the FTIR spectrum of the Zn-doped Li $[Li_{0.20}Mn_{0.54}Ni_{0.13}Co_{0.13-x}Zn_x]\ O_2$ cathode with x = 0.02, the peaks related to TM-O bonds observed in Figure 2a were also clearly present. Figure 2c shows the FTIR spectrum of the Zn-doped Li $[Li_{0.20}Mn_{0.54}Ni_{0.13}Co_{0.13-x}Zn_x]\ O_2$ cathode with x = 0.05. In addition to the absorption bands assigned to

© 2026 *The Author(s).*

CC BY 4.0

TM-O bonds, a broad peak appeared around 3500 cm^{-1}. This peak can be attributed to O-H stretching vibrations, most likely originating from adsorbed moisture on the sample surface rather than being intrinsic to the cathode structure [17, 18].

Field-emission scanning electron microscopy (FE-SEM) analysis is a useful characterization technique for examining surface morphology and particle size. Figure 3a presents the FESEM image of the undoped Li $[Li_{0.20}Mn_{0.54}Ni_{0.13}Co_{0.13}]\ O_2$ cathode. The image shows agglomerated polyhedral nanostructures. These nanostructured particles are associated with the Li $[Li_{0.20}Mn_{0.54}Ni_{0.13}Co_{0.13}]\ O_2$ cathode material, and most of them have sizes below 100 nm .

As shown in Figure 3b, which presents the FESEM image of the Zn-doped Li $[Li_{0.20}Mn_{0.54}Ni_{0.13}Co_{0.13-x}Zn_x]\ O_2$ cathode with x = 0.02, the agglomerated polyhedral nanostructured particles observed in Figure 3a were also evident. The incorporation of Zn into the Li-rich cathode framework did not noticeably alter the morphological characteristics. Similarly, the FESEM image of the Zn-doped Li $[Li_{0.20}Mn_{0.54}Ni_{0.13}Co_{0.13-x}Zn_x]\ O_2$ cathode with x = 0.05, shown in Figure 3c, exhibited morphology similar to that of the undoped and x = 0.02 samples. This suggests that increasing the Zn dopant concentration did not substantially affect the overall morphology of the cathode particles.

The elemental composition of the samples was analyzed using energy-dispersive X-ray spectroscopy (EDXS). Figure 4a shows the EDXS spectrum of the undoped Li $[Li_{0.20}Mn_{0.54}Ni_{0.13}Co_{0.13}]\ O_2$ cathode. The EDXS spectra of the Zn -doped Li $[Li_{0.20}Mn_{0.54}Ni_{0.13}Co_{0.13-x}Zn_x]\ O_2$ cathodes with x = 0.02 and x = 0.05, shown in Figures 4b and 4c, respectively, exhibit peaks corresponding to Ni, Mn, Co, and O, which originate from the cathode material. In addition to these peaks, Zn peaks were detected in the doped samples, confirming the incorporation of Zn into the cathode composition. The elemental compositions of the samples are presented in Tables 2-4.

Raman spectroscopy was used to investigate the structural changes caused by Zn doping in the Li-rich cathode material. Figure 5a shows the Raman spectrum of the undoped Li $[Li_{0.20}Mn_{0.54}Ni_{0.13}Co_{0.13}]\ O_2$ cathode recorded over the range of 0 – 3500 cm^{-1}. A sharp peak was clearly observed at approximately 500 cm^{-1}.

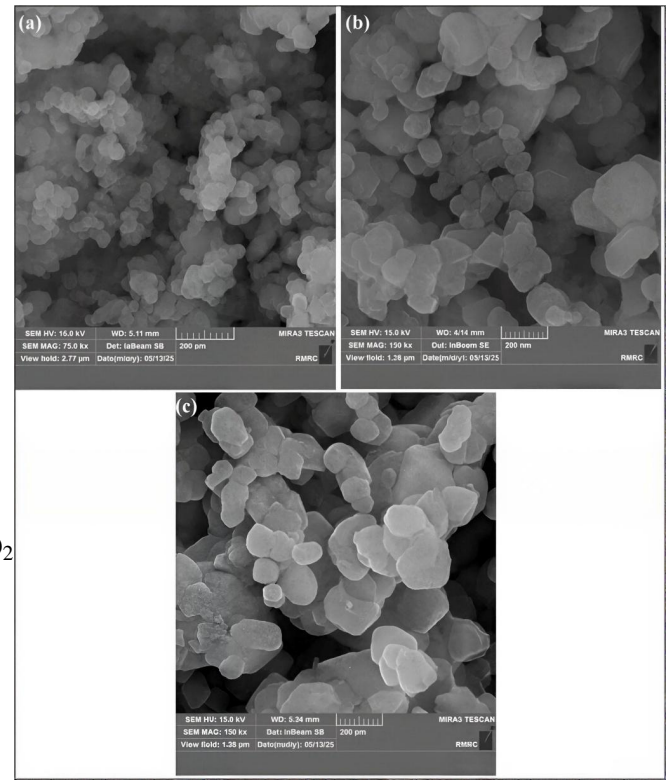

Fig. 3 FESEM images taken for (a) undoped Li $[Li_{0.20}Mn_{0.54}Ni_{0.13}Co_{0.13-x}Zn_x]\ O_2$ cathode (x = 0) and the ones doped with Zn dopant where (b) x = 0.02 and (c) x = 0.05.

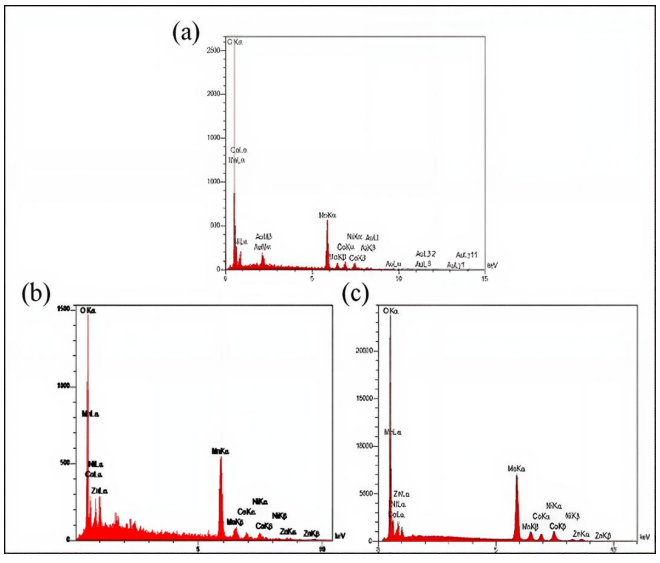

Fig. 4 the EDXS patterns of (a) the undoped Li $[Li_{0.20}Mn_{0.54}Ni_{0.13}Co_{0.13-x^2}Zn_x]\ O_2$ cathode (x = 0) and (b) and (c) the ones doped with Zn, where x = 0.02 and x = 0.05, respectively.

© 2026 *The Author(s).* CC BY 4.0

Table 2 Elemental composition of undoped Li $[Li_{0.20}Mn_{0.54}Ni_{0.13}Co_{0.13-x}Zn_x]$ O_2 cathode (x = 0).

Elt	Line	Int	Error	W K	W Kr	W%	A%
0	Ka	651.8	3.9962	0.4405	0.3687	47.15	75.79
Mn	Ka	396.2	0.6853	0.3844	0.3217	35.76	16.74
Co	Ka	56.4	0.7025	0.0819	0.0685	8.14	3.55
Ni	Ka	50.8	0.7111	0.0932	0.0780	8.95	3.92
				1.0000	0.8370	100.00	100.00

Table 3 Elemental composition of doped Li $[Li_{0.20}Mn_{0.54}Ni_{0.13}Co_{0.13-x}Zn_x]$ O_2 cathode (x = 0.02).

Elt	Line	Int	Error	K	Kr	W%	A%
O	Ka	374.8	7.0960	0.2933	0.1776	47.67	48.80
Mn	Ka	391.6	0.8018	0.4399	0.2663	35.17	11.76
Co -	Ka	24.8	0.8219	0.0418	0.0253	7.39	1.09
Ni	Ka	33.3	0.8320	0.0707	0.0428	7.59	1.80
Zn	Ka	7.7	0.8522	0.0285	0.0173	2.18	0.69
				1.0000	0.6053	100.00	100.00

Table 4 Elemental composition of doped Li $[Li_{0.20}Mn_{0.54}Ni_{0.13}Co_{0.13-x}Zn_x]$ O_2 cathode (x = 0.05).

Elt	Line	Int	Error	K	Kr	W%	A%
O	Ka	771.4	7.8070	0.1965	0.1629	27.52	58.89
Mn	Ka	1464.7	1.3557	0.5356	0.4439	47.29	29.47
Co	Ka	117.2	1.3898	0.0641	0.0531	5.99	3.48
Ni	Ka	143.3	1.4069	0.0991	0.0821	8.87	5.17
Zn	La	292.5	1.2868	0.1046	0.0867	10.33	2.98
				1.0000	0.8287	100.00	100.00

According to previous studies, this peak corresponds to the A_1 g mode, which is associated with the symmetric stretching vibration of transition metal-oxygen (TM-O) bonds in the cathode structure [3, 7].

The incorporation of different Zn dopant concentrations into the Li $[Li_{0.20}Mn_{0.54}Ni_{0.13}Co_{0.13-x}Zn_x]$ O_2 cathode resulted in changes in the Raman peak observed in Figure 5a, including peak broadening and a shift toward a higher Raman shift. As shown in Figures 5b and 5c, which present the Raman spectra of the Zn-doped Li-rich cathodes with x = 0.02 and x = 0.05, respectively, the peaks corresponding to TM-O bonds were clearly observed.

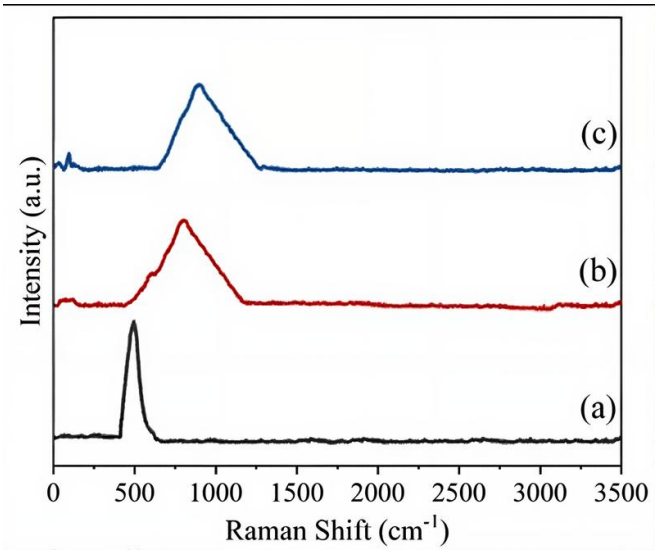

Fig. 5 Raman spectra of (a) undoped Li $[Li_{0.20}Mn_{0.54}Ni_{0.13}Co_{0.13-x}Zn_x]_{02}$ cathode (x = 0) and the ones doped with Zn dopant where (b)x = 0.02 and (c)x = 0.05.

3.2 Electrochemical analyses

Cyclic voltammetry (CV) measurements were performed to investigate the redox activity of the synthesized undoped and Zn-doped samples. Figure 6a shows the CV curve of the undoped Li $[Li_{0.20}Mn_{0.54}Ni_{0.13}Co_{0.13}]$ O_2 cathode recorded over the voltage range of 2.0 – 5.0 V versus Li/Li^+. The anodic peak observed at approximately 4.2 V is associated with lithium-ion deintercalation from the cathode, accompanied by oxidation of the transition-metal species. The cathodic peak observed at approximately 3.8 V is attributed to lithium-ion intercalation into the cathode, accompanied by reduction of the transition-metal species.

The anodic and cathodic peaks observed at 4.2 and 3.8 V, respectively, are mainly assigned to the $Ni^{2+}/Ni^{3+}/Ni^{4+}$ redox reaction, because Mn^{4+} ions are generally electrochemically inactive in this voltage range, whereas Co^{3+}/Co^{4+} redox reactions usually occur at voltages above 4.6 V. The peaks related to the O^{2-}/O^{-} oxygen redox reaction, which also contributes to the capacity of Lirich cathodes, were not clearly detected in Figure 6a, as they typically appear at voltages above 4.4 V versus Li/Li^+ [3, 19].

© 2026 *The Author(s).*

CC BY 4.0

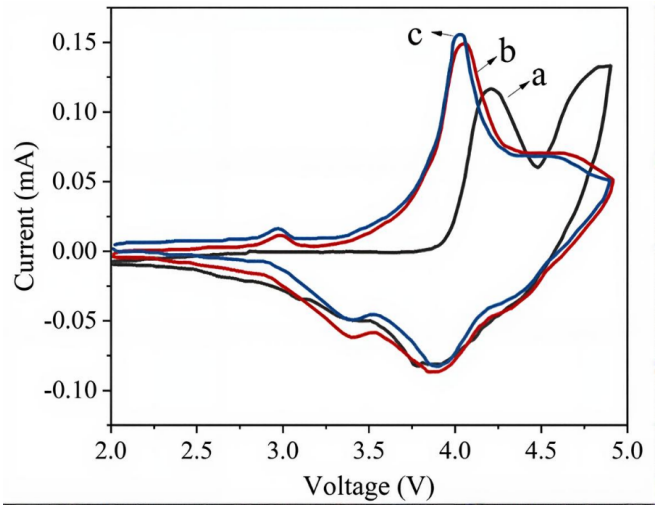

Fig. 6 CV diagrams recorded for (a) undoped Li $[Li_{0.20}Mn_{0.54}Ni_{0.13}Co_{0.13-x}Zn_x]\ O_2$ cathode ($x = 0$) and the ones doped with Zn dopant where (b) x = 0.02 and (c) x = 0.05.

In the CV curves of the Zn-doped Li $[Li_{0.20}Mn_{0.54}Ni_{0.13}Co_{0.13-x}Zn_x]\ O_2$ cathodes with x = 0.02 (Figure 6b) and x = 0.05 (Figure 6c), the redox peaks corresponding to the $Ni^{2+}/Ni^{3+}/Ni^{4+}$ reaction were clearly observed. However, compared with the undoped sample, a slight shift in peak position was observed. In addition to the peak shift, the redox peak intensity was also affected by Zn doping. Compared with the undoped cathode, the Zn-doped samples showed higher peak intensity, which is consistent with the Rietveld refinement results. As shown in Table 1, Zn doping slightly expanded the lattice parameters, which may facilitate lithium-ion intercalation and deintercalation at the cathode. Consequently, the redox peaks became more intense and the polarization decreased.

Figure 7 shows the Nyquist plots of the undoped Li $[Li_{0.20}Mn_{0.54}Ni_{0.13}Co_{0.13}]\ O_2$ cathode and its Zn-doped counterparts with different Zn concentrations. The equivalent circuit shown in the inset of Figure 7 was used to fit the EIS spectra.

The semicircular feature observed in the mid-frequency region represents the charge-transfer resistance, denoted as Rct in Figure 7, which is associated with Li^+ ion transfer at the electrode/electrolyte interface. The inclined linear region observed at low frequency corresponds to Warburg impedance (Zw), which reflects lithium-ion diffusion within the electrode material. The solution resistance is labeled as Re, whereas the constant phase element is denoted as CPE. Re represents the ohmic resistance of the cell, mainly arising from the ionic conductivity of the electrolyte, separator, and current collectors. It is typically observed in the high-frequency region of the Nyquist plot [20–23]. Table 5 summarizes the parameters obtained from fitting the Nyquist plots.

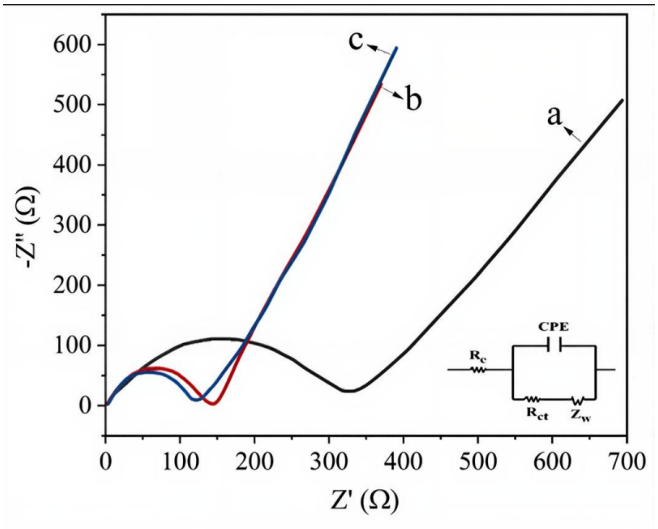

Fig. 7 EIS diagrams demonstrating (a) the undoped Li $[Li_{0.20}Mn_{0.54}Ni_{0.13}Co_{0.13-x}Zn_x]\ O_2$ cathode (with x = 0) and those featuring the Zn dopant, specifically (b) when x = 0.02 and (c) when x = 0.05. (The inset illustrates the equivalent circuit used for fitting the Nyquist plots).

Table 5 R_e, R_{ct}, and Z_W of the dopant-free Li $[Li_{0.20}Mn_{0.54}Ni_{0.13}Co_{0.13-x}Zn_x]\ O_2$ cathode (x = 0) alongside its variants doped with varying amounts of Zn.

Sample	$R_e(\Omega)$	$R_{ct}(\Omega)$	$Z_W(\Omega)$
Pure	6.6	317.4	0.79
Pure + Zn (x = 0.02)	2.8	135	0.69
Pure + Zn (x = 0.05)	3.6	118	0.65

In this regard, the undoped Li $[Li_{0.20}Mn_{0.54}Ni_{0.13}Co_{0.13}]O_2$ cathode exhibited an Rct value of 317.4 Ω. The introduction of different Zn concentrations resulted in a marked reduction in Rct. Specifically, the Rct values of the Zn -doped Li $[Li_{0.20}Mn_{0.54}Ni_{0.13}Co_{0.13-x}Zn_x]\ O_2$ cathodes with x = 0.02 and x = 0.05 were 135 and 118Ω, respectively, which were much lower than that of the undoped sample. Clearly, increasing the Zn dopant content substantially reduced Rct. Similar to the charge-transfer resistance, Zn doping also decreased Re.

The introduction of Zn also influenced the Warburg impedance. Compared with the undoped sam-

© 2026 *The Author(s).*

CC BY 4.0

ple, the Zn-doped cathodes exhibited lower Zw values. The lowest Zw value was observed for the Zn -doped Li $[Li_{0.20}Mn_{0.54}Ni_{0.13}Co_{0.13-x}Zn_x]\,O_2$ cathode with x = 0.05, reaching 0.65Ω. The EIS results were in good agreement with the CV analysis, indicating that Zn doping reduced polarization, which was consistent with the increased intensity of the redox peaks.

The initial charge-discharge characteristics of the undoped Li $[Li_{0.20}Mn_{0.54}Ni_{0.13}Co_{0.13}]\,O_2$ cathode and its Zn-doped counterparts are shown in Figure 8.

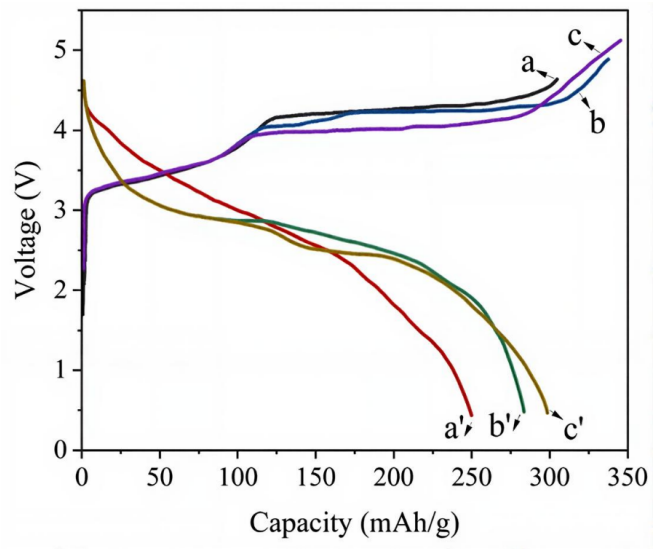

Fig. 8 The initial charge and discharge cycle for the dopant-free Li $[Li_{0.20}Mn_{0.54}Ni_{0.13}Co_{0.13}-\ x^{Zn}JO_2$ cathode is shown in (a,a'), along with the changes observed with Zn doping, specifically in (b,b') where x = 0.02, and in (c, c′) where x = 0.05. The galvanostatic evaluations were performed at a rate of 0.1 C within the voltage range of 1.8 to 4.8 V .

According to Table 6, the $Li[Li_{0.20}Mn_{0.54}Ni_{0.13}Co_{0.13-x}Zn_x]O_2$ cathode with $x = 0.05$ exhibited the best electrochemical performance. This sample delivered a charge capacity of 345.4 mAh g^{-1}, a discharge capacity of 298.7 mAh g^{-1}, and a Coulombic efficiency (CE) of 86.5%. The higher charge and discharge capacities of the Zn-doped cathodes compared with the undoped sample can be attributed to the role of Zn doping in expanding the lattice parameters, facilitating lithium-ion diffusion, and reducing electrochemical resistance.

To compare the electrochemical performance of the synthesized cathodes with those reported in the literature, Table 7 presents the charge capacity, discharge capacity, and CE values of different cathode materials. Overall, the Zn-doped cathode prepared in this study showed electrochemical performance comparable to that of previously reported cathode materials.

Table 6 The charge capacity, discharge capacity, and Coulombic efficiency of the dopant-free Li $[Li_{0.20}Mn_{0.54}Ni_{0.13}Co_{0.13-x}Zn_x]\,O_2$ cathode ($x = 0$) are presented, along with its variants that have been doped with differing concentrations of Zn.

Sample	Charge Capacity (mAh/g)	Discharge Capacity (mAh/g)	CE (%)
Pure	304.7	249.8	81.9
Pure + Zn ($x = 0.02$)	337.6	283.6	84
Pure + Zn ($x = 0.05$)	345.4	298.7	86.5

Table 7 Comparison of electrochemical performance of our cathode with other works, which were recorded after the 1st cycle. The pure cathode in all the investigated references was Li $[Li_{0.20}Mn_{0.54}Ni_{0.13}Co_{0.13}]\,O_2$.

Dopant	Coating agent	Voltage (V)	C-rate	Charge Capacity (mAh/g)	Discharge Capacity (mAh/g)	CE (%)	Ref.
Nb	-	2.0-4.8	0.1	343.2	267.7	78	[24]
Mo	ZrF_4	2.0-4.8	0.1	350.6	270.6	77.1	[25]
Al and In	-	2.0-4.8	0.1	~325	~275	84.6	[26]
Zn	-	1.8-4.8	0.1	345.4	298.7	86.5	Our work

The findings of this study highlight that even a small amount of Zn doping (x = 0.02–0.05) can markedly improve the electrochemical performance of lithium- and manganese-rich cathodes. Compared with previous reports that used higher Zn contents or alternative dopants, such as Mg and Nb, the present results show that low-level Zn substitution is sufficient to expand the lattice, reduce charge-transfer resistance, and enhance lithium-ion diffusion pathways. This directly addresses the existing research gap regarding the role of Zn in stabilizing layered cathodes at low concentrations. By providing evidence that minor Zn incorporation can preserve structural integrity while enhancing electrochemical activity, this study advances the understanding of Zn doping and offers a promising approach for designing next-generation cathode materials.

© 2026 *The Author(s).*

CC BY 4.0

4 CONCLUSION

In this study, undoped Li $[Li_{0.20}Mn_{0.54}Ni_{0.13}Co_{0.13}]$ O_2 cathodes and Zn -doped Li $[Li_{0.20}Mn_{0.54}Ni_{0.13}Co_{0.13-x}Zn_x]$ O_2 cathodes with different Zn concentrations were successfully synthesized. XRD analysis showed that all samples, including the undoped and Zn-doped cathodes, retained a similar layered $\alpha - NaFeO_2$ structure. The presence of TM-O vibrational bands in the FTIR spectra further supported the successful synthesis of the materials. Raman spectra of the undoped and Zn-doped cathodes exhibited the A_1 g vibration mode of TM-O bonds. Polyhedral nanostructured particles were observed in the FESEM images of all cathodes, indicating that Zn doping had minimal effect on the morphology of the cathode nanoparticles.

According to CV and EIS analyses, Zn doping reduced electrochemical resistance, which may be related to lattice expansion and improved lithium-ion transport. The enhanced charge-transfer kinetics observed in the EIS results suggest that Zn plays an important role in lowering interfacial impedance, thereby enabling faster lithium-ion migration and more efficient redox activity. The Li $[Li_{0.20}Mn_{0.54}Ni_{0.13}Co_{0.08}Zn_{0.05}]$ O_2 cathode, corresponding to x = 0.05, demonstrated a charge capacity of 345.4mAhg^{-1}, a discharge capacity of 298.7mAhg^{-1}, and a Coulombic efficiency of 86.5%. These findings indicate that Zn-doped lithium- and manganeserich layered oxides are promising cathode materials for next-generation lithium-ion batteries, particularly for applications requiring improved capacity and reduced interfacial resistance.

Funding source

No funds received.

Data availability

N/A

DECLARATIONS

Conflict of interest

The authors declare no competing interests

Consent to publish

N/A

Ethical approval

N/A

REFERENCES

[1] Goodenough JB, Park KS. The Li-Ion Rechargeable Battery: A Perspective. Journal of the American Chemical Society. 2013;135(4):1167-76. 10.1021/ja3091438

[2] Tarascon JM, Armand M. Issues and Challenges Facing Rechargeable Lithium Batteries. Nature. 2001;414(6861):359-67. 10.1038/35104644

[3] Zhao S, Yan K, Zhang J, Sun B, Wang G. Reaction Mechanisms of Layered Lithium-Rich Cathode Materials for High-Energy Lithium-Ion Batteries. Angewandte Chemie International Edition. 2021;60(5):2208-20. 10.1002/anie.202000262

[4] Darjazi H, Rezvani SJ, Brutti S, Nobili F. Improvement of Structural and Electrochemical Properties of NMC Layered Cathode Material by Combined Doping and Coating. Electrochimica Acta. 2022;404:139577. 10.1016/j.electacta.2021.139577

[5] Nitta N, Wu F, Lee JT, Yushin G. Li-Ion Battery Materials: Present and Future. Materials Today. 2015;18(5):252-64. 10.1016/j.mattod.2014.10.040

[6] Yan J, Huang H, Tong J, Li W, Liu X, Zhang H, et al. Recent Progress on the Modification of High Nickel Content NCM: Coating, Doping, and Single Crystallization. Interdisciplinary Materials. 2022;1(3):330-53. 10.1002/idm2.12043

[7] Çetin B, Camtakan Z, Yuca N. Synthesis and Characterization of Li-Rich Cathode Material for Lithium-Ion Batteries. Materials Letters. 2020;273:127927. 10.1016/j.matlet.2020.127927

[8] Zhang K, Sheng H, Wu X, Fu L, Liu Z, Zhou C, et al. Improving Electrochemical Properties by Sodium Doping for Lithium-Rich Layered Oxides. ACS Applied Energy Materials. 2020;3(9):8953-9. 10.1021/acsaem.0c01402

[9] Hendrickx M, Paulus A, Kirsanova MA, Van Bael MK, Abakumov AM, Hardy A, et al. The Influence of Synthesis Method on the Local Structure and Electrochemical Properties of Li-Rich/Mn-Rich NMC Cathode Materials for Li-Ion Batteries. Nanomaterials. 2022;12(13):2269. 10.3390/nano12132269

[10] Jeong S, Park S, Park J, Beak M, Lee J, Kwon EE, et al. The Enhancement of Cyclability of Ni-Rich $LiNi_{0.9}Co_{0.05-x}Mn_{0.05}Zn_x$ Cathode Materials by the Substitution of Zn for Co. International Journal of Energy Research. 2022;46(13):19177-89. 10.1002/er.8178

© 2026 *The Author(s).*

CC BY 4.0

[11] Shi Y, Kim K, Xing Y, Millonig A, Kim B, Wang L, et al. Facile and Scalable Dry Surface Doping Technique to Enhance the Electrochemical Performance of $LiNi_{0.64}Mn_{0.2}Co_{0.16}O_2$ Cathode Materials. Journal of Materials Chemistry A. 2020;8(38):19866-72. 10.1039/D0TA07779H

[12] Sanad MMS, Meselhy NK, El-Boraey HA, Toghan A. Controllable Engineering of New $ZnAl_2O_4$-Decorated $LiNi_{0.8}Mn_{0.1}Co_{0.1}O_2$ Cathode Materials for High-Performance Lithium-Ion Batteries. Journal of Materials Research and Technology. 2023;23:1528-42. 10.1016/j.jmrt.2023.01.102

[13] Vanaphuti P, Chen J, Cao J, Bigham K, Chen B, Yang L, et al. Enhanced Electrochemical Performance of the Lithium-Manganese-Rich Cathode for Li-Ion Batteries with Na and F Codoping. ACS Applied Materials & Interfaces. 2019;11(41):37842-9. 10.1021/acsami.9b13838

[14] Ahmed BR, Reyhani A, Khanlary MR, Mortazavi SZ. Investigation of the Synergetic Effects of GO and Zn on the Electrochemical Properties of $Li[Li_{0.20}Mn_{0.54}Ni_{0.13}Co_{0.13}]O_2$ Cathode Material. Chemical Methodologies. 2025;9(9):737-50. 10.48309/chemm.2025.509286.1912

[15] Farshori NN, Al-Oqail MM, Al-Sheddi ES, Al-Massarani SM, Saquib Q, Siddiqui MA, et al. Green Synthesis of Silver Nanoparticles Using Phoenix dactylifera Seed Extract and Its Anticancer Effect Against Human Lung Adenocarcinoma Cells. Journal of Drug Delivery Science and Technology. 2022;70:103260. 10.1016/j.jddst.2022.103260

[16] Echegaray-Ugarte TS, Cespedes-Loayza AL, Cruz-Loayza JL, Huayapa-Yucra LA, Cruz I, de Carvalho JC, et al. Green Synthesis of Silver Nanoparticles Mediated by Punica granatum Peel Waste: An Effective Additive for Natural Rubber Latex Nanofibers Enhancement. Polymers. 2024;16(11):1531. 10.3390/polym16111531

[17] Ikemoto Y, Harada Y, Tanaka M, Nishimura Sn, Murakami D, Kurahashi N, et al. Infrared Spectra and Hydrogen-Bond Configurations of Water Molecules at the Interface of Water-Insoluble Polymers under Humidified Conditions. The Journal of Physical Chemistry B. 2022;126(22):4143-51. 10.1021/acs.jpcb.2c01702

[18] Dai F, Zhuang Q, Huang G, Deng H, Zhang X. Infrared Spectrum Characteristics and Quantification of OH Groups in Coal. ACS Omega. 2023;8(19):17064-76. 10.1021/acsomega.3c01336

[19] Hashem AM, Abdel-Ghany AE, Scheuermann M, Indris S, Ehrenberg H, Mauger A, et al. Doped Nanoscale NMC333 as Cathode Materials for Li-Ion Batteries. Materials. 2019;12(18):2899. 10.3390/ma12182899

[20] Yavarinasab A, Abedini M, Tahmooressi H, Janfaza S, Tasnim N, Hoorfar M. Potentiodynamic Electrochemical Impedance Spectroscopy of Polyaniline-Modified Pencil Graphite Electrodes for Selective Detection of Biochemical Trace Elements. Polymers. 2022;14(1):31. 10.3390/polym14010031

[21] Kim C, Jang I. Application of Electrochemical Impedance Spectroscopy for Diagnostics in Fuel Cells, Electrolyzers, and Batteries. ChemElectroChem. 2025;12(11):e202500005. 10.1002/celc.202500005

[22] Kasper M, Moertelmaier M, Ragulskis M, Al-Zubaidi R-Smith N, Angerer J, Aufreiter M, et al. Calibrated Electrochemical Impedance Spectroscopy and Time-Domain Measurements of a 7 kWh Automotive Lithium-Ion Battery Module with 396 Cylindrical Cells. Batteries & Supercaps. 2023;6(2):e202200415. 10.1002/batt.202200415

[23] Celeste A, Brescia R, Gigli L, Plaisier JR, Pellegrini V, Silvestri L, et al. Unravelling Structural Changes of the $Li_{1.2}Mn_{0.54}Ni_{0.13}Co_{0.13}O_2$ Lattice upon Cycling in Lithium Cell. Materials Today Sustainability. 2023;21:100277. 10.1016/j.mtsust.2022.100277

[24] Xu Y, Cui Q. Nb-Doped $Li_{1.20}[Mn_{0.54}Ni_{0.13}Co_{0.13}]O_2$ Cathode Material with Enhanced Electrochemical Properties for Lithium-Ion Batteries. International Journal of Electrochemical Science. 2020;15(1):803-15. 10.20964/2020.01.47

[25] Lu Y, Shi S, Yang F, Zhang T, Niu H, Wang T. Mo-Doping for Improving the ZrF_4-Coated $Li[Li_{0.20}Mn_{0.54}Ni_{0.13}Co_{0.13}]O_2$ as High-Performance Cathode Materials in Lithium-Ion Batteries. Journal of Alloys and Compounds. 2018;767:23-33. 10.1016/j.jallcom.2018.07.068

[26] Bai R, Zhao Y, Lu C, Meng Y, Gao W, Wang Y, et al. Sonochemical Synthesis and Electrochemical Performance of Reduced Graphene Oxide/Cerium Dioxide Nanocomposites. Journal of Chemical Research. 2023;47(2):17475198231158745. 10.1177/17475198231158745

© 2026 *The Author(s).*

CC BY 4.0

How to cite this article

Khadem RJ. Improving the Electrochemical Performance of Lithium- and Manganese-Rich Layered Cathodes Through Low-Level Zinc Doping . Journal of University of Anbar for Pure Science. 2026; 20(2):232-242. doi:10.37652/juaps.2026.164769.1664

© 2026 *The Author(s).*

CC BY 4.0